

# 低介電常數材料在多層導體連線系統上之製程 整合研究

研究生：蔡宗鳴

指導教授：曾俊元博士

張鼎張博士

國立交通大學

電子工程學系 電子研究所



當元件尺寸進入奈米領域 (<100 nm)時，訊號傳輸的電阻-電容時間延遲 (RC delay time)是現今多層金屬連線製程技術急需解決的問題。為了克服這一個問題，在內層金屬連線結構中使用金屬銅導線與低介電常數材料是一個不錯的方法。然而當低介電常數材料與銅導線製程整合時，將面臨到不同於昔知製程技術的挑戰。所以本論文將研究四種極具潛力的低介電常數材料：Methylsilsequiazane (MSZ)，Porous Polysilazane (PPSZ)，Hydrogen Silsesquioxane (HSQ)，以及 Porous Organosilicate Glass (POSG)，並對其所遇到之製程整合問題提出相關的解決方法。

在傳統的多層導體連線微影製程中，去除光阻的步驟是無法避免的。而在去除光阻的過程中，氧電漿灰化是主要的製程方式。本論文發現氧電漿會造成低介

電常數材料介電特性的劣化，而且實驗結果顯示多孔性的低介電常數材料比一般的低介電常數材料更容易被氧電漿破壞。這是因為多孔性的低介電常數材料有較大的表面面積，所以氧電漿容易擴散入材料中，並與材料中的官能基(如甲基鍵等)反應形成 Si-OH 鍵結，而這些極性鍵結很容易吸附外界的水氣，進而造成介電特性的劣化。為了防止低介電常數材料在光阻去除過程中受到傷害，本文採用在氧電漿處理前利用 H<sub>2</sub> 與 NH<sub>3</sub> 電漿處理，使其在低介電常數材料上形成鈍化層以防止後續氧電漿的破壞。實驗結果顯示此方法是可行的。另外，對於低介電常數材料在光阻處理過程中所產生的 Si-OH 鍵結，也可以用 trimethylchlorosilane (TMCS)與 hexamethyldisilazane (HMDS)的化學處理方式置換成 Si-O-SiMe<sub>3</sub> 的疏水性原子團，並有效的恢復被氧電漿所破壞的介電特性。

為了能夠進一步將銅導線與低介電常數材料整合在一起，鑲嵌式的銅導線結構是目前極為可行的製程方式。而在此製程中，化學機械磨製程(CMP)將扮演非常重要的角色。但是隨著晶片(chip)的功能越來越強大，其電路佈局的複雜性與積集度也日益增加，使得 CMP 的終點偵測日益困難，因此本論文將研究國家奈米實驗室(NDL)所提供的 TaN 與 Cu 研磨液在 CMP 製程中對低介電常數材料介電特性的影響。實驗結果顯示此兩種研磨液並不會對 MSZ 與 PPSZ 材料的介電特性有任何的影響，而且其對這兩種材料的研磨速度也比 TaN 與 Cu 金屬低很多。因此利用此兩種低介電常數材料於銅導線製程中可以使終點偵測比較容易，且其介電特性在此 CMP 製程中不會受到影響。另外，在電性可靠度分析上，本研究也發現 MSZ 與 PPSZ 材料與銅金屬有良好的可靠度，因此 MSZ 與 PPSZ 材料在鑲嵌式銅導線製程的應用上是很有潛力的。

由於金屬沉積前介電層(PMD)的低溫化與平坦化的要求日益重要，使得低介電常數材料的 CMP 平坦化製程有探討的必要性。本論文發現利用傳統的矽酸鹽類研磨液(SS-25)不能對 MSZ 或 PPSZ 產生高的研磨率，因此吾人提出利用氧電漿處理的方法來增加含有甲基的 MSZ 與 PPSZ 薄膜之研磨率。氧電漿可以在 MSZ 或 PPSZ 薄膜表面形成一親水層進而提高 SS-25 研磨液對此低介電常數材料的研

磨率，而且一旦此親水層被磨除後，此低介電常數材料就會被恢復到原本的低介電特性。

此外，為了避免去除光阻製程對低介電常數材料的傷害，以及符合下一代微影製程的要求，本論文亦提出一種利用電子束(e-beam)對低介電常數材料直接圖形化的技術。此技術是利用電子束的能量使低介電常數材料固化，然後再利用適當的溶劑進行圖形的顯影以得到想要的電路圖案。研究發現此技術確實可以運用於低介電常數材料的圖形化，但需要在圖形化製程後多一道熱退火的製程才能得到理想的低介電常數材料特性。

在對多孔性 POSG 低介電常數材料進行 e-beam 直接圖形化的實驗中，吾人發現此材料經過電子束照射，顯影製程與後續熱退火製程後，其介電常數竟然比傳統熱爐管固化的 POSG 薄膜要來的低。經過實驗的分析得知，可能的原因是由於電子束照射只能使 POSG 材料產生局部的網路連結(crosslink)，所以在顯影過程中部分未連結的聚合單體會被顯影液所帶走而留下孔洞，因此經過熱退火製程後其薄膜的孔隙度會比傳統的熱爐管固化材料還要來的高，導致出現更低的介電常數值。而在漏電傳導機制的研究中，發現電子束的照射會使 POSG 材料的漏電機制由原本熱爐管固化 POSG 的 Schottky emission 傳導機制轉變成 Space-charge-limited current 的傳導機制。

# The Process Integration of Low-k Dielectrics for Multilevel Interconnection Applications

**Student: Tsung-Ming Tsai**

**Advisor: Dr. Tseung-Yuen Tseng  
Dr. Ting-Chang Chang**

**Department of Electronic Engineering and Institute of Electronics**

**College of Electrical Engineering and Computer Science**

**National Chiao Tung University**



Although the dimension of device has shrunk into nano technology node, the RC delay of inter-metal interconnection has still been the urgent issue needed to be resolved so far. In order to overcome this problem, the introduction of low-dielectric-constant (low-k) material for inter-metal interconnection can effectively reduce the RC delay. However, it is necessary to estimate the compatibility of low-k materials on semiconductor process during the integration of Cu and low-k materials. In this dissertation, four types of low-k materials are investigated: Methylsilsequiazane (MSZ), Porous Polysilazane (PPSZ), Hydrogen Silsesquioxane (HSQ), and Porous Organosilicate Glass (POSG).

In the traditional lithography process for integrated circuit manufacture, photoresist removal step is an inevitable process. O<sub>2</sub> plasma ashing is the main method to remove the photoresist during photoresist (PR) stripping process. It was found that the oxygen plasma will degrade the dielectric properties of low-k material.

We have found that the porous low-k materials are more easily damaged by O<sub>2</sub> plasma than that of dense low-k materials. This reason is that the porous low-k materials have larger exposed surface area than that of dense low-k materials. As a result, the oxygen radical can easily diffuse into material and react with the functional group, such as methyl bonding, which is converted to Si-OH bonds. These polar chemical bonding can lead to moisture uptake under atmosphere, resulting in dielectric degradation. In order to prevent the low-k materials from O<sub>2</sub> plasma damage during photoresist stripping process, H<sub>2</sub> and NH<sub>3</sub> plasma treatments were applied to low-k materials before PR stripping process. These plasma treatments can effectively form a passivation layer on the surface of low-k materials and protect the low-k materials from O<sub>2</sub> plasma damage. Besides, the Si-OH formed from O<sub>2</sub> plasma ashing process can also be eliminated by trimethylchlorosilane (TMCS) and hexamethyldisilazane (HMDS) post-treatment. These chemical treatment can change the hydrophilic Si-OH into hydrophobic Si-O-Si(CH<sub>3</sub>)<sub>3</sub> bonds so that the dielectric characteristics of low-k materials can be recovered.

In order to integrate the Cu and low-k materials into multilevel interconnection, the Cu damascene structure has been accepted to be a promising architecture up to now. In this process, the chemical mechanical polishing (CMP) technology will impersonate a critical role. However, with the functionality of chip is more powerful, the complexity and density of circuit layout are increased more significantly. This will cause the end point detection of CMP process more difficultly. Therefore, there are two slurries (TaN and Cu slurries), which is provided by national nano device laboratory (NDL), used to investigate the impact of CMP process on dielectric properties of low-k materials. It was found that these two slurries can not influence the dielectric properties of MSZ and PPSZ during CMP processes. Moreover, the selectivity of Cu or TaN with respect to MSZ and PPSZ films is high as polished by

Cu or TaN slurries. Therefore, manufacturing Cu interconnect using the two low-k materials can make the end point detection easily and do not influence the dielectric properties during CMP processes. In addition, it was found that the electrical reliability of Cu and these two materials can be remained under reliability test. Therefore, the application of MSZ and PPSZ for Cu damascene structure has a lot of potential.

In virtue of the requirement of low thermal budget and high planarization for pre-metal dielectric (PMD) is gradually significant in future, it is necessary to investigate the CMP of low-k materials in this study. The experimental results represent that the high polishing rate of MSZ or PPSZ can not be obtained by using commercial silica-based SS-25 slurry. Therefore, O<sub>2</sub> plasma pretreatment on low-k materials is proposed to improve the polishing rate of low-k materials. The O<sub>2</sub> plasma can react with MSZ or PPSZ to form a hydrophilic layer, which will raise the polishing rate of methyl contained MSZ or PPSZ films with SS-25 slurry. Moreover, the dielectric properties of these low-k materials can be maintained as the hydrophilic layer was polished away.

In addition, a novel electron beam (e-beam) direct patterning technology is proposed so as to avoid the damage during photoresist removal process. The e-beam energy can provide energy to cure the low-k materials from mono-polymer structure into network structure. Then, the uncured region of low-k materials can be dissolved by suitable developer. After development process, the desirable pattern can be obtained by this technology. But an additional thermal annealing is needed to achieve the required low-k dielectric properties.

During the experiment of e-beam direct patterning on porous POSG film, it was found that the dielectric constant of e-beam exposed POSG after development and thermal annealing processes is lower than that of traditional furnace cured one. The

possible reason is that the e-beam exposure can only partially crosslink the POSG films. Once the e-beam exposed POSG is subjected to developer, the uncrosslinked polymer of POSG will be taken away, resulting in the pore in POSG films. After the thermal annealing process, the porosity of film will be higher than that of traditional furnace cured one. In addition, the leakage current behavior of e-beam exposed POSG film is investigated. After e-beam exposure, there are many charge trapping sites remained in POSG films, which will cause local potential barrier height and affect the carriers transport in POSG film. Electrical analyses reveal that the behavior of leakage conduction mechanism of POSG will be from Schottky emission transferred into Space-Charge-Limited Current (SCLC).



## 誌謝

時光飛逝，歲月如梭，隨著論文寫作的完成，亦代表著我即將從交通大學完成博士學位，心中對許多人、事、物的萬分謝意，實在是意長紙短，不知如何在此文中完整表達。在交大博士班的修業期間，首先要特別感謝我的兩位指導教授——曾俊元教授及張鼎張教授，在這兩位教授多年來的教誨與鼓勵下，本論文才能順利的完成。曾俊元教授在研究上給我很寬廣的發揮空間，並適時的給予我啟發與鼓勵，令學生受益匪淺。在待人處世上，曾教授圓融的處事態度及認真為學的精神，讓學生獲益良多。另外，張鼎張教授對我論文研究的指導更是不遺餘力，不僅指引我論文的研究方向，當研究遇到瓶頸時，張教授也會用心的協助學生突破難關。此外，張教授積極處事的態度與學術上高瞻遠矚的創見，亦是學生努力追求的典範。能夠師承兩位師長，是我畢生的榮幸，對於兩位老師的感激之情，實難用筆墨來形容。

再者，由衷的感謝亦師亦友的劉柏村教授對我這些年來論文的指正與建議，除了實驗上的設計外，劉教授對論文寫作技巧上的協助，更讓我順利的完成論文寫作。在此，學生要對劉教授致上最誠摯的謝意。同時也要感謝羅正忠教授、崔秉鉞教授、聯華電子盧火鐵協理、工研院電子所張啟明經理在百忙之中撥空參加口試擔任委員，並對我的論文提供意見與指導，使我的論文更加的完備，由衷的感謝您們。

另外，也要謝謝交大半導體中心與國家奈米元件實驗室提供良好的研究設備與環境，使實驗能順利的完成。亦感謝秘書林詩融小姐在實驗與行政上的協助與幫忙，希望林小姐可以永保青春美麗。

博士論文並不是靠一己之力就可以完成的，還要感謝曾經和我一起日以繼夜奮鬥的學長、學弟妹們：小莫、紀文、碩廷、政桓、曉琪、若慈、宗衛、鴻明、阿娟、蓓欣、小杰、元均、靜宜、子軒、炳麟、世仰，沒有你們的幫忙與扶持，我的論文沒辦法完成；另外，也要感謝仍在實驗室奮鬥的學弟們：炳宏、致宏、



敏全、土撥、國王、興華、泓緯、大山，有你們陪伴我渡過這艱辛的博士班歲月，心中滿是感激。我會永遠記得跟大家一起在路邊攤把酒言歡的日子，謝謝你們。還有實驗室的同伴們：仁宏、永俊、志益、群傑、思毅及所有的碩士班學弟妹，有你們的鼓勵，使我有力量堅持到最後，謝謝你們。要感謝的人實在太多了，可能有遺漏，但對你們的謝意是不會少的。

最後，我要感謝上天給我如此良好的環境，感謝我的父母親，無怨無悔的供我讀書，讓年近三十的我能無後顧之憂的完成博士班學業，希望我能以這一點點殊榮讓他們得到片刻的喜悅。

僅將此文獻給所有關心我的老師、家人與親友



蔡 宗 鳴  
誌於 風城交大  
2005 年 初春

# Contents

<b>Chinese Abstract</b>	-----	i
<b>English Abstract</b>	-----	iv
<b>Acknowledgment</b>	-----	viii
<b>Contents</b>	-----	x
<b>Table Captions</b>	-----	xii
<b>Figure Captions</b>	-----	xiii
<b>Chapter 1 Introduction</b>		
1.1 General Background	-----	1
1.2 Organization of the dissertation	-----	11
<b>Chapter 2 Study on the impact of plasma treatment and CMP process on low-k Methylsilsequiazane (MSZ) for interconnection applications</b>		
2.1 Introduction	-----	26
2.2 Experimental Procedures	-----	27
2.3 Results and Discussions	-----	33
2.4 Conclusion	-----	42
<b>Chapter 3 The effect of CMP process on ultra low-k porous-polysilazane (PPSZ) for ULSI application</b>		
3.1 Introduction	-----	68
3.2 Experimental Procedures	-----	69
3.3 Results and Discussions	-----	72
3.4 Conclusion	-----	79

<b>Chapter 4</b>	<b>Study on Direct Pattern Method of Low-k Hydrogen Silsesquioxane (HSQ) Using Electron Beam Lithography Technology</b>	
4.1	Introduction	97
4.2	Experimental Procedures	98
4.3	Results and Discussions	99
4.4	Conclusion	103
<b>Chapter 5</b>	<b>Study on the Feasibility of Electro-Beam Direct Patterning on Low-k MSZ for Interconnection Applications</b>	
5.1	Introduction	113
5.2	Experimental Procedures	114
5.3	Results and Discussions	115
5.4	Conclusion	118
<b>Chapter 6</b>	<b>Exploration of the Effect of Electron Beam Curing on Organic Ultra Low-k Porous Organosilicate Glass (POSG) Material</b>	
6.1	Introduction	124
6.2	Experimental Procedures	125
6.3	Results and Discussions	127
6.4	Conclusion	134
<b>Chapter 7</b>	<b>Conclusions and Suggestions for Future Work</b>	
7.1	Conclusions	149
7.2	Suggestions for future work	154
<b>References</b>		155
<b>Vita</b>		169
<b>Publication List</b>		170

# Table Captions

## *Chapter 1*

Table 1-1 The requirements for low-k dielectrics.

Table 1-2 Basic intrinsic properties of several low-k materials.

Table 1-3 MPU interconnect technology requirements-Near-term.

Table 1-4 MPU interconnect technology requirements-Long-term.

## *Chapter 2*

Table 2-1 The conditions of H<sub>2</sub>, NH<sub>3</sub>, and O<sub>2</sub> plasma treatments for Methylsilsequiazane (MSZ).

Table 2-2 The parameters of CMP process.



## Figure Captions

### *Chapter 1*

- Fig. 1-1 The RC delay trend of nano-scaled ULSI circuits. (Source: ITRS 2003)
- Fig. 1-2 The architecture of multilevel interconnect metallization.
- Fig. 1-3 The cross-section of interconnect system with parasitic capacitance.
- Fig. 1-4 Foam Formation Process (Source: K. R. Carter, IBM Research Division, 1997)
- Fig. 1-5 Typical process flow of Cu damascene architecture integrated with low-k material.
- Fig. 1-6 The planarization flow of PMD with CMP process.
- Fig. 1-7 Lithography Exposure Tool Potential Solutions.
- Fig. 1-8 Photoresist stripping processes during the fabrication of damascene structure.
- Fig. 1-9 Scheme of e-beam direct patterning of low-k dielectrics for the manufacture of dual damascene structure.  
Regions I are uncured low-k materials in a gel-like state and  
Regions II are crossed-linked state after e-beam exposure.

### *Chapter 2*

- Fig. 2-1 Formation mechanism of MSZ film.
- Fig. 2-2 FTIR spectra of MSZ film during formation.
- Fig. 2-3 The internal stress variation of MSZ film during thermal cycle.
- Fig. 2-4 FTIR spectra of MSZ films after various anneal temperature.
- Fig. 2-5 Dielectric properties of the MSZ film after thermal annealed at various temperature (a) leakage current density of the MSZ versus electric field. (b) Dielectric constant of the MSZ films versus annealing temperature.

Fig. 2-6 The leakage current density of (a) temperature and (b) time dependence of thermal stress for Cu electrode MIS structure.

Fig. 2-7 FTIR spectra of MSZ film after O<sub>2</sub> plasma treatment for 3 to 9 minutes.

Fig. 2-8 The TDS moisture desorption spectra of O<sub>2</sub> plasma-treated MSZ films.

Fig. 2-9 Dielectric properties of MSZ after O<sub>2</sub> plasma treatment.

(a) leakage current density of MSZ versus electric field

(b) dielectric constant of MSZ versus O<sub>2</sub> plasma treatment time.

Fig.2-10 FTIR spectra of as-cured and H<sub>2</sub> plasma-treated 3 min films after undergoing O<sub>2</sub> plasma treatment.

Fig. 2-11 Dielectric properties of as-cured and H<sub>2</sub> plasma-treated 3 min films after undergoing O<sub>2</sub> plasma treatment (a) leakage current density of MSZ films versus electric field (b) Dielectric constant of the MSZ films.

Fig. 2-12 FTIR spectra of as-cured and NH<sub>3</sub> plasma-treated 3 min films after undergoing O<sub>2</sub> plasma treatment.

Fig. 2-13 Dielectric properties of as-cured and NH<sub>3</sub> plasma-treated 3 min films after undergoing O<sub>2</sub> plasma treatment (a) leakage current density of the MSZ films versus electric field (b) Dielectric constant of the MSZ films.

Fig. 2-14 FTIR spectra of MSZ films with O<sub>2</sub> plasma and subsequent TMCS/HMDS treatment.

Fig. 2-15 Thickness variation of MSZ films with O<sub>2</sub> plasma and subsequent TMCS/HMDS treatment.

Fig. 2-16 Dielectric properties of MSZ films with O<sub>2</sub> plasma and subsequent TMCS/HMDS treatment (a) leakage current density of the MSZ versus electric field (b) dielectric constant of the MSZ.

Fig. 2-17 AFM image surface of polished MSZ (a) with TaN slurry (b) with Cu slurry.

- Fig. 2-18 AFM micrograph surface of polished MSZ with commercial SS-25 slurry.
- Fig. 2-19 FTIR Spectra of post-CMP MSZ with various slurries.
- Fig. 2-20 Dielectric properties of polished MSZ with various slurries. (a) leakage current density of post-CMP MSZ versus electric field (b) dielectric constant of post-CMP MSZ films.
- Fig. 2-21 Removal rate of CMP for MSZ with and without O<sub>2</sub> plasma pre-treatment.
- Fig. 2-22 AFM micrographs of 1 min O<sub>2</sub> plasma-treated MSZ films (a) without CMP process (b) with CMP process.
- Fig. 2-23 FTIR spectra of O<sub>2</sub> plasma-treated MSZ films before and after CMP process.
- Fig. 2-24 Moisture-desorption spectra of O<sub>2</sub> plasma-treated MSZ films before and after CMP process.
- Fig. 2-25 The auger depth profile of (a) as-cured and (b) 1 min O<sub>2</sub> plasma treated MSZ film.
- Fig. 2-26 Dielectric properties of O<sub>2</sub> plasma-treated MSZ before and after CMP process (a) leakage current density of MSZ films as a function of electric field (b) variation in dielectric constant of O<sub>2</sub> plasma-treated MSZ films.
- Fig. 2-27 Leakage-current density of sample O before and after the 150 °C bake [curve I, sample STD measured at 25 °C; curve II, sample O measured at 25 °C (before 150 °C bake); curve III, sample O measured at 150 °C; curve IV, sample O measured at 25 °C (after 150 °C bake)].
- Fig 2-28 Leakage-current density of sample C before and after 150 °C bake [curve I, sample STD measured at 25 °C; curve II, sample C measured at 25 °C (before 150 °C bake); curve III, sample C measure at 150 °C; curve IV, sample C measured at 25 °C (after 150 °C bake)].

### ***Chapter 3***

- Fig. 3-1 Method of precursor structure transfer to final porous-polysilazane (PPSZ) structure.
- Fig. 3-2 FTIR spectra of PPSZ film during formation.
- Fig. 3-3 The internal stress variation of PPSZ during thermal cycle.
- Fig. 3-4 FTIR spectra of PPSZ films after various thermal annealing temperature.
- Fig. 3-5 Dielectric properties of the PPSZ film after thermal annealed at various temperature (a) leakage current density of the PPSZ versus electric field (b) dielectric constant of the PPSZ films versus annealing temperature.
- Fig. 3-6 The leakage current density of temperature dependence of thermal stress for Cu electrode MIS structure.
- Fig. 3-7 Comparison of leakage current density of PPSZ before and after BTS stress at 190 °C and 2 MV/cm for 1000 sec.
- Fig. 3-8 J-E curves performed with different sweeping times. It is found that the leakage current is decreased with increasing sweeping times.
- Fig. 3-9 AFM image surface of polished PPSZ (a) with TaN slurry (b) with Cu slurry.
- Fig. 3-10 AFM micrograph surface of polished PPSZ with commercial SS-25 slurry.
- Fig. 3-11 FTIR Spectra of post-CMP PPSZ with various slurries.
- Fig. 3-12 Dielectric properties of PPSZ films polished with various slurries: (a) leakage current density of post-CMP PPSZ films versus electric field (b) dielectric constants of post-CMP PPSZ films.
- Fig. 3-13 The TDS moisture desorption spectra of PPSZ polished with various slurries



- Fig. 3-14 Leakage current density of Cu-electrode polished PPSZ film after 2 MV/cm at 150 °C for 1000 sec BTS stress measured at room temperature and 150 °C (a) with SS-25 Slurry (b) with TaN Slurry (c) with Cu slurry.
- Fig.3-15 Removal rate of CMP with and without O<sub>2</sub> plasma pre-treatment.
- Fig. 3-16 AFM micrographs of 30 sec O<sub>2</sub> plasma-treated PPSZ films (a) without CMP process (b) with CMP process.
- Fig. 3-17 FTIR spectra of O<sub>2</sub> plasma-treated PPSZ films before and after CMP process.
- Fig. 3-18 The auger depth profile of (a) as-cured PPSZ film and (b) 45 sec O<sub>2</sub> plasma treated PPSZ film.
- Fig. 3-19 Dielectric properties of O<sub>2</sub> plasma-treated PPSZ before and after CMP process (a) leakage current density of PPSZ films versus electric field (b) variation in dielectric constant of PPSZ films.
- Fig. 3-20 Leakage-current density of sample O before and after the 150 °C bake [curve I, sample STD measured at 25 °C; curve II, sample O measured at 25 °C (before 150 °C bake); curve III, sample O measured at 150 °C; curve IV, sample O measured at 25 °C (after 150 °C bake)].
- Fig. 3-21 Leakage-current density of sample C before and after 150 °C bake [curve I, sample STD measured at 25 °C; curve II, sample C measured at 25 °C (before 150 °C bake); curve III, sample C measure at 150 °C; curve IV, sample C measured at 25 °C (after 150 °C bake)].

## ***Chapter 4***

- Fig. 4-1 Traditional lithography process for the fabrication of damascene structure.
- Fig. 4-2 Proposed e-beam lithography process for the fabrication of damascene structure.
- Fig. 4-3 FTIR spectra of HSQ during traditional thermal baking and furnace

curing processes

- Fig. 4-4 The cage-like and network-like structure of HSQ.
- Fig. 4-5 FTIR spectra of HSQ films with different doses of electron beam exposure, ranging from 100  $\mu\text{C}/\text{cm}^2$  to 700  $\mu\text{C}/\text{cm}^2$ .
- Fig. 4-6 The leakage current densities of e-beam exposed HSQ films at different doses.
- Fig. 4-7 Dielectric constant of e-beam exposed HSQ films at different doses.
- Fig. 4-8 The SEM cross-sectioned profile of collapsed pattern for dense HSQ lines.
- Fig. 4-9 The possible scenario of pattern collapse for dense HSQ lines.
- Fig. 4-10 The SEM micrograph of patterned HSQ film with critical dimensions of 60 nm.
- Fig. 4-11 The comparison of dielectric constants of e-beam exposed HSQ films with different treatment.
- Fig. 4-12 Leakage current of e-beam exposed HSQ with TMAH development followed by thermal annealing, as compared to typical furnace cured HSQ films.
- Fig. 4-13 Temperature dependence of moisture desorption from HSQ films with e-beam exposed HSQ followed by TMAH developed and thermal annealed processes and with furnace curing.

## ***Chapter 5***

- Fig. 5-1 The thickness variation of e-beam exposed MSZ films with different doses.
- Fig. 5-2 FITR spectra of e-beam exposed MSZ films with different doses.

Fig. 5-3 The leakage current of e-beam exposed MSZ is compared to that of traditional furnace cured one.

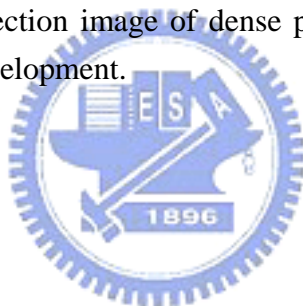
Fig. 5-4 The FTIR spectra of e-beam exposed MSZ with different doses after thermal annealing.

Fig. 5-5 Dielectric properties of e-beam exposed MSZ with different doses after thermal annealing (a) leakage current density of MSZ films versus electric field (b) variation in dielectric constant of MSZ films

Fig. 5-6 The transfer curve of e-beam exposed MSZ with different doses after 10 % wt TMAH development process.

Fig. 5-7 The optical image of single line pattern of e-beam exposed MSZ film after development.

Fig. 5-8 The SEM cross section image of dense pattern lines of e-beam exposed MSZ film after development.



## **Chapter 6**

Fig 6-1 Proposed e-beam direct patterning process.

Fig 6-2 The FTIR spectra of as-spun POSG film after a series of bake and furnace curing steps.

Fig 6-3 The brief diagram of POSG formation procedures.

Fig 6-4 FTIR spectra of POSG films after O<sub>2</sub> plasma ashing for 30 to 90 sec.

Fig 6-5 Dielectric properties of POSG after O<sub>2</sub> plasma ashing for 30 to 90 sec (a) leakage current density of POSG films versus electric field (b) dielectric constant of post-treated POSG films.

Fig 6-6 The variation of refractive index of POSG films with electron exposed doses from 2 uC/cm<sup>2</sup> to 810 uC/cm<sup>2</sup>.

- Fig 6-7 The remained thickness of the POSG film with different doses after development.
- Fig 6-8 FTIR spectra of POSG films with different doses of electron beam exposure.
- Fig. 6-9 The leakage current densities of e-beam exposed POSG films at different doses.
- Fig. 6-10 Dielectric constant of e-beam exposed POSG films at different doses.
- Fig. 6-11 The leakage current densities of e-beam exposed POSG films at different doses with furnace annealing process.
- Fig. 6-12 The dielectric constant of e-beam exposed POSG films at different doses with furnace annealing process.
- Fig. 6-13 The SEM image of patterned wafer after e-beam curing and development processes without post-exposure annealing.
- Fig. 6-14 The FTIR spectra of POSG films with e-beam exposure and followed by development and post-thermal annealing treatments.
- Fig. 6-15 The proposed model for the decrease of dielectric constant on the e-beam exposed POSG after development and subsequent thermal annealing processes. (a) e-beam direct patterning process (b) traditional furnace curing process.
- Fig. 6-16 The leakage current density of e-beam exposed POSG films with 8  $\mu\text{C}/\text{cm}^2$  dosage after undergoing various treatment.
- Fig. 6-17 The dielectric constant of e-beam exposed POSG films with 8  $\mu\text{C}/\text{cm}^2$  dosage after undergoing various treatment.
- Fig. 6-18 The leakage current behavior of furnace cured POSG film.
- Fig. 6-19 The band diagram of schottky emission mechanism for a metal/furnace cured POSG/Si capacitor.

Fig. 6-20 The leakage current density of e-beam exposed POSG film measured at different temperature.

Fig. 6-21 The current fitting of e-beam exposed POSG film at room temperature.

Fig. 6-22 The current fitting of e-beam exposed POSG film at 150 °C.

Fig. 6-23 The band diagram of space charge limit current mechanisms for e-beam exposed POSG MIS structure.

